Title
Does vapor pressure deficit drive the seasonality of δ13C of the net land-atmosphere CO2 exchange across the United States?

Journal
Journal of Geophysical Research Biogeosciences, 122(8)

ISSN
2169-8953

Authors
Raczka, B
Biraud, SC
Ehleringer, JR
et al.

Publication Date
2017-08-01

DOI
10.1002/2017jg003795

Peer reviewed

Does vapor pressure deficit drive the seasonality of $\delta^{13}C$ of the net land-atmosphere CO_2 exchange across the United States?

B. Raczka

S. C. Biraud

J. R. Ehleringer

C.-T. Lai

J. B. Miller

D. E. Pataki

S. R. Saleska

M. S. Torn
B. H. Vaughn

R. Wehr

D. R. Bowling
First published: 22 July 2017

https://doi.org/10.1002/2017JG003795

Cited by: 1
UC-eLinks

Abstract

The seasonal pattern of the carbon isotope content ($\delta^{13}C$) of atmospheric CO_2 depends on local and nonlocal land-atmosphere exchange and atmospheric transport. Previous studies suggested that the $\delta^{13}C$ of the net land-atmosphere CO_2 flux (δ_{source}) varies seasonally as stomatal

conductance of plants responds to vapor pressure deficit of air (VPD). We studied the variation of δ_{source} at seven sites across the United States representing forests, grasslands, and an urban center. Using a two-part mixing model, we calculated the seasonal δ_{source} for each site after removing background influence and, when possible, removing $\delta^{13}C$ variation of nonlocal sources. Compared to previous analyses, we found a reduced seasonal (March–September) variation in δ_{source} at the forest sites (0.5‰ variation). We did not find a consistent seasonal relationship between VPD and δ_{source} across forest (or other) sites, providing evidence that stomatal response to VPD was not the cause of the global, coherent seasonal pattern in δ_{source}. In contrast to the forest sites, grassland and urban sites had a larger seasonal variation in δ_{source}(5‰) dominated by seasonal transitions in C_3/C_4 grass productivity and in fossil fuel emissions, respectively. Our findings were sensitive to the location used to account for atmospheric background variation within the mixing model method that determined δ_{source}. Special consideration should be given to background location depending on whether the intent is to understand site level dynamics or regional scale impacts of land-atmosphere exchange. The seasonal amplitude in $\delta^{13}C$ of land-atmosphere CO_2exchange (δ_{source}) varied across land cover types and was not driven by seasonal changes in vapor pressure deficit. The largest seasonal amplitudes of δ_{source} were at grassland and urban sites, driven by changes in C_3/C_4 grass productivity and fossil fuel emissions, respectively. Mixing model approaches may incorrectly calculate δ_{source} when background atmospheric observations are remote and/or prone to anthropogenic influence.

1 Introduction

The land-atmosphere exchange of carbon has an important influence on the magnitude and spatiotemporal pattern of both the mole fraction and $\delta^{13}C$ of atmospheric CO_2. The global average atmospheric CO_2 mole fraction increased by ~40% from 1850 to 2016 (from 280 to 400 ppm) primarily driven by fossil fuel emissions. Concurrently, the $\delta^{13}C$ of atmospheric CO_2 (δ_{atm}) has decreased [*Rubino et al.*, 2013] and continues to decrease at a rate of −0.25‰ per decade in the northern midlatitudes [*Bowling et al.*, 2014]. The δ_{atm} is also influenced by land and ocean processes [*Randerson et al.*, 2002; *Alden et al.*, 2010], predominantly through photosynthetic discrimination by land plants [*Farquhar et al.*, 1989] (vegetation assimilates $^{12}CO_2$ at a higher rate than for $^{13}CO_2$) and also because the $\delta^{13}CO_2$ of the carbon absorbed and released by the land and ocean systems, respectively, are in isotopic disequilibrium. The terrestrial biosphere discriminates against $^{13}CO_2$ (^{13}C hereafter) relative to $^{12}CO_2$ (^{12}C hereafter) by 12–16‰ on average [*Fung et al.*, 1997; *Suits et al.*, 2005], which is much larger than the discrimination by the net ocean exchange (2.0‰). This difference in discrimination allows the use of observations of δ_{atm} to constrain the global carbon budget and partition the global carbon uptake between the land and ocean through atmospheric inversion modeling [*Ciais et al.*, 1995; *Battle et al.*, 2000; *Alden et al.*, 2010]. Many of these modeling approaches, however, assume that the photosynthetic discrimination by land plants is constant, despite evidence to the contrary [e.g., *Randerson et al.*, 2002; *Scholze et al.*, 2003; *van der Velde et al.*, 2013]. Relatively small uncertainties in

photosynthetic discrimination can introduce large uncertainties in inferred carbon uptake. For example, just a 1‰ decrease in photosynthetic discrimination results in a direct increase in the inferred land uptake of 0.2 Pg C yr^{-1} [*Still et al.*, 2003a]. Uncertainty in discrimination can also indirectly influence land-ocean carbon partitioning through the inferred land isotopic disequilibrium, which is important for balancing the global isotopic carbon budget. In this case, just a 0.1‰ decrease in photosynthetic discrimination can affect the inferred land uptake by 0.7 Pg C yr^{-1}[*Randerson*, 2005]. These uncertainties in the inferred land uptake are as much as 27% of the total annual carbon uptake by the global land carbon sink [*Le Quéré et al.*, 2015]. Therefore, the uncertainty of terrestrial ^{13}C discrimination inhibits an accurate diagnosis of the atmospheric and land conditions that impact the global carbon budget.

The terrestrial ^{13}C discrimination is primarily influenced through isotopic fractionation during C_3 photosynthesis [*Farquhar et al.*, 1989]. Photosynthesis dominates global land-atmosphere exchange of carbon during the summer causing the troposphere to become enriched in ^{13}C (δ_{atm} less negative) as a result of net carbon uptake by plants, followed by a decrease in δ_{atm} (more negative) during the winter due to a net release of depleted, plant-derived carbon. The $\delta^{13}C$ of respiration (δ_{resp}) is similar but not identical to photosynthetic uptake (δ_{photo}) because of age-driven isotopic disequilibrium (Suess effect) and post-photosynthetic fractionation processes [*Bowling et al.*, 2008; *Brüggemann et al.*, 2011]. The magnitude of photosynthetic discrimination is controlled by the balance of CO_2 supply and demand in the chloroplast. The supply of CO_2 depends primarily on stomatal conductance, which responds to environmental conditions. In general, plants reduce their stomatal conductance during environmental conditions unfavorable for photosynthesis, and thus, δ_{photo} responds to atmospheric moisture deficit, soil water content, precipitation, and nutrient availability [*Farquhar et al.*, 1989; *Bowling et al.*, 2008; *Cernusak et al.*, 2013].

An improved understanding of environmental conditions that influence stomatal conductance and δ_{source} (through δ_{photo}) is important for the parameterization of terrestrial carbon models. For example, the coupling of the carbon and water cycles through plant stomata has been represented through the Ball-Berry [*Ball et al.*, 1987] and Leuning [*Leuning*, 1995] models. Previous site-level studies have demonstrated that the Leuning model outperforms the Ball-Berry model due to the dependence upon vapor pressure deficit (VPD) and relative humidity of air for each model, respectively [e.g., *Nijs et al.*, 1997; *Way et al.*, 2011; *Prentice et al.*, 2014]. In addition, global land surface modeling has suggested that the Leuning model better represents seasonal changes in δ_{source}, as compared to the Ball-Berry [*Ballantyne et al.*, 2011]. It was unclear, however, whether this improved performance was a result of the mechanistic linkage between stomatal

conductance and VPD or from including more parameters within the model. This distinction can provide an important difference for carbon cycle projections given the diverging paths of VPD and relative humidity under future climate scenarios [*Sato et al.*, 2015] and the impact on the strength of the terrestrial carbon sink [*Arora et al.*, 2013]. Furthermore, terrestrial carbon models have been parameterized with stable carbon isotopes and have showed promise in calibrating parameters that influence stomatal conductance (e.g., stomatal slope) [*Aranibar et al.*, 2006; *Raczka et al.*, 2016]. Thus, the estimation of seasonal changes in δ_{source} has the potential to provide an important test and guidance for terrestrial carbon model development.

One approach to understand land-atmosphere exchange of $\delta^{13}C$ (δ_{source}) takes advantage of site-level measurements of atmospheric CO_2 and δ_{atm}. This approach estimates δ_{source}through a two-part mixing model that assumes that the local atmospheric CO_2 mole fraction and δ_{atm} are from a combination of background (nonlocal) and local sources. Several types of mixing models have been developed; however, the Miller-Tans plot [*Miller and Tans*, 2003] with background correction [*Ballantyne et al.*, 2010] is generally the most robust method, capable of accounting for time-varying background influences. All mixing models have limited applicability to when there is a single, well-mixed local net source or sink [*Vardag et al.*, 2016].

Mixing models have been used to identify several factors that contribute to variation in δ_{resp}. First, short-term changes in environmental conditions have been linked to changes in δ_{resp}. For example, stomatal response to VPD influences the $\delta^{13}C$ of soil [*Ekblad and Högberg*, 2001] or whole-forest respiration, and in some conifer forests, there is a 10–15 day lag time for the highest correlation between VPD and δ_{resp} [*Bowling et al.*, 2002]. Soil moisture has been found to be correlated with δ_{resp} at Howland and Wind River sites [*Lai et al.*, 2005] and precipitation at sites across North and South America [*Pataki et al.*, 2003b]. Linkages between VPD and soil moisture with δ_{resp}, however, are not universal [*Schaeffer et al.*, 2008; *Riveros-Iregui et al.*, 2011; *Shim et al.*, 2011; *Bowling et al.*, 2014]. The cause of seasonal variation of δ_{source} is less well understood, but it has been hypothesized that the coherent seasonal pattern in δ_{source} among midlatitude sites (coniferous forest, deciduous forest, and crops) inferred from an atmospheric mixing model is driven by stomatal response to seasonal variation in VPD [*Ballantyne et al.*, 2010, 2011].

Second, strong seasonality in δ_{source} occurs in mixed C_3/C_4 grasslands, caused by a seasonal transition from primarily C_3 photosynthesis during spring/early summer to a varying mixture of C_3/C_4 photosynthesis during mid/late summer [*Lai et al.*, 2003; *Still et al.*, 2003b; *Torn et al.*, 2011]. Grasslands are prevalent worldwide [*Collatz et al.*, 1998] and thus an important contributor to the seasonality of global δ_{atm} [*Fung et al.*, 1997; *Conte and Weber*, 2002; *Still et al.*, 2003a]. Although natural mixtures of C_3/C_4 grasslands have become increasingly rare due to

land-use change from agriculture [*Torn et al.*, 2011], the regional planting of a combination of C_3/C_4 crops (corn (C_4), soybean (C_3), and wheat (C_3)) likely have similar impacts upon regional δ_{source} and δ_{atm} due to atmospheric mixing. For example, an analysis of tall tower observations taken over fields of mostly corn and soybeans in the upper Midwest found that δ_{atm} was dominated by C_3 discrimination during the spring and fall; however, C_4 species accounted for as much as 45% of the gross photosynthetic flux during summer [*Griffis et al.*, 2010]. Third, urban areas can impose a local seasonal cycle in δ_{source}reflecting the type and emission rate of fossil fuels. For example, the seasonal cycle of δ_{source}in Salt Lake City is influenced by high emissions from natural gas combustion during winter (for heating), by plant and soil CO_2 exchange during summer, and by petroleum combustion (transportation) year-round [*Pataki et al.*, 2003a, 2007]. In this case, the depleted $\delta^{13}C$ signature of CO_2 from combustion of natural gas as compared to petroleum and biogenic respiration creates a seasonal δ_{source} that is relatively depleted in the winter and enriched during the summer. These three mechanisms—VPD influencing stomatal conductance and δ_{photo}, C_3/C_4 grassland transition, and fossil fuel emission with seasonal changes in fuel type—each, alone, or in combination, contribute to observed seasonal changes in both $\delta_{source}$and δ_{atm}. The relative importance of these three mechanisms both locally and regionally remains unclear.

Here we analyze atmospheric observations from seven sites within the United States to determine the seasonality of δ_{source}. Departing from previous studies, we account for nonlocal influences by choosing a background location that is nearly collocated with the site of interest to isolate the local (~1–10 km^2) δ_{source} signal. We examine to what extent the choice of background location and temporal resolution affect δ_{source}. We choose sites that together provide over 50 site-years of atmospheric observations and include coniferous forest, deciduous forest, grassland, and an urban site to understand how land type influences δ_{source} and δ_{atm}. Specifically, we test the hypothesis of *Ballantyne et al.* [2011] that the coherent seasonal cycle in δ_{source} among midlatitude sites is driven primarily by plant stomatal conductance responding to seasonal changes in VPD. Finally, we use the isoforcing, a function of the site-level δ_{source} and the net carbon exchange (NEE), to determine what factors are most responsible for the seasonal change in the $\delta^{13}C$ of net land-atmosphere exchange of CO_2 and how this may impact δ_{atm}.

2 Materials and Methods

This section describes the observation sites (section 2.1) and observation protocol (section 2.2) used for this analysis and a description of the methods used to calculate the δ_{source}(section 2.3) and isoforcing (section 2.4) for each site. This is followed by a description of the method used to

diagnose the influence of VPD (section 2.5) and anthropogenic trace gases (section 2.6) on δ_{source}. A complete list of variables is provided in Table 1.

Table 1. List of Variables Used

Symbol	Description	Unit or Unit Symbol
C_a	Atmospheric mole fraction of CO_2 at site location	ppm
C_{av}	Atmospheric concentration of CO_2	μmol m^{-3}
C_{bg}	Atmospheric mole fraction of CO_2 at background location	ppm
C_{source}	Local contribution (addition or removal) of atmospheric CO_2	ppm
$C_{smoothbg}$	Background CO_2 using *smoothed* method	ppm
$C_{nonsmoothbg}$	Background CO_2 using *nonsmoothed* method	ppm
$\delta^{13}C$	$^{13}C/^{12}C$ isotope composition (relative to VPDB)	‰
δ_{atm}	$\delta^{13}C$ of atmospheric CO_2	‰
δ_a	$\delta^{13}C$ of CO_2 at site location	‰
δ_{bg}	$\delta^{13}C$ of CO_2 at background location	‰

Symbol	Description	Unit or Unit Symbol
δ_{resp}	$\delta^{13}C$ of ecosystem respiration	‰
δ_{photo}	$\delta^{13}C$ of net photosynthetic assimilation	‰
$\delta_{smoothbg}$	Background $\delta^{13}C$ (*smoothed* method)	‰
$\delta_{smoothsource}$	Local $\delta^{13}C$ of land-atmosphere exchange of CO_2 (*smoothed* method)	‰
$\delta_{nonsmoothbg}$	Background $\delta^{13}C$ (*nonsmoothed* method)	‰
$\delta_{nonsmoothsource}$	Local $\delta^{13}C$ of land-atmosphere exchange of CO_2 (*nonsmoothed* method)	‰
δ_{source}	Local $\delta^{13}C$ of land-atmosphere exchange of CO_2	‰
δ_{wood}	$\delta^{13}C$ of tree ring cellulose	‰
Isoforcing	Influence of net land carbon exchange upon δ_{atm}	‰ µmol m s^{-1}
$\sigma_{\delta source}$	Uncertainty of δ_{source}	‰
NEE	Net ecosystem exchange of carbon	µmol m^{-2} s^{-1}
GPP	Gross primary productivity (gross photosynthesis)	µmol m^{-2} s^{-1}

Symbol	Description	Unit or Unit Symbol
VPD	Vapor pressure saturation deficit of air	kPa
VPDB	Vienna Pee Dee Belemnite standard for $\delta^{13}C$	‰

2.1 Site Description

The sites (Table 2) represent a variety of land cover types including evergreen forests (*US-NR1*, Wind River, Howland), deciduous forests (Harvard), grasslands (*SGP*, Rannells), and an urban area (Salt Lake City). *US-NR1* is a subalpine conifer forest located in the Rocky Mountains of Colorado. The site is a secondary growth forest and consists of lodgepole pine (*Pinus contorta*), Engelmann spruce (*Picea engelmannii*), and subalpine fir (*Abies lasiocarpa*) [*Monson et al.*, 2002; *Hu et al.*, 2010a]. The Wind River site is located within Gifford Pinchot National Forest, Washington, and is an old-growth temperate conifer forest dominated by Douglas fir (*Pseudotsuga menziesii*) and western hemlock (*Tsuga heterophylla*) [*Shaw et al.*, 2004; *Unsworth et al.*, 2004]. The Howland site is located within a boreal-northern hardwood forest about 50 km north of Bangor, Maine. Land cover is dominated by conifers of red spruce (*Picea rubens*), eastern hemlock (*Tsuga canadensis*), and lesser amounts of red maple (*Acer rubrum*) and paper birch (*Betula papyrifera*) [*Richardson et al.*, 2009]. The Harvard site is a temperate deciduous forest outside of Petersham, Massachusetts dominated by red oak (*Quercus rubra*) and red maple (*Acer rubrum*) with lesser coverage of hemlock (*T. canadensis*) and red pine (*Pinus resinosa*) [*Urbanski et al.*, 2007]. The Southern Great Plains (*SGP*) site is located in Lamont, Oklahoma where land cover is a mixture of grassland (used for pasture and grazing) and annual crops, mainly winter wheat. In general, C_3 photosynthesis dominates during the early spring whereas both C_3 and C_4 grass species are active during summer. The Rannells site, near Manhattan, Kansas, is similar to *SGP* in that it is a mixture of C_3 and C_4 grasses [*Lai et al.*, 2006]. There were no eddy covariance flux tower data available at Rannells; therefore, NEE from the nearby Konza prairie (*US-Kon*) was used to estimate ^{13}C isoforcing (section 2.4). *US-Kon* is located approximately 5 km from Rannells with similar vegetation and environmental conditions [*Turner et al.*, 2003]. The Salt Lake City observations were made on the roof of a building at the University of Utah campus located 3.5 km east of downtown [*Pataki et al.*, 2003a, 2007].

Table 2. Description of the Sites and Methods for the Atmospheric CO_2 and $\delta^{13}C$ Observations

Site Name (Manuscript Designation)	Network (AmeriFlux, NOAA, DOE-ARM Site Codes)	Location (Degrees Lat. Long.)	Sampling Frequency	Sampling Method	Years	Sampling Heights (m)	Vegetation
Harvard	AmeriFlux (*US-Ha1*)	(42.54, −72.17)	Flask and continuous	Flask: *Lai et al.* [2005]; Continuous: *Wehr et al.*[2013]	2001–2009; 2011–2014	0.1, 0.2, 22.4; 0.2, 1, 7.5, 12.5, 18.3, 24.1, 29	Deciduous forest
Howland	AmeriFlux (*US-Ho1*)	(45.20, −68.74)	Flask	*Lai et al.*[2005]	2001–2009	0.4, 9.3, 24.7	Boreal evergreen forest
Niwot Ridge (forest: US-NR1) (tundra: NWR)	AmeriFlux (*US-NR1*) *NOAA* (*NWR*)	(Forest: 40.03, −105.55); (tundra: 40.05, −105.63)	Continuous (forest) and flask (tundra)	Continuous: *Bowling et al.* [2014]: aFlask	2006–2014; a1990–2014	0.1, 0.5, 1, 2, 5, 7, 9, 11, 21.5	Temperate evergreen forest
Rannells Flint Hills Prairie (Rannells)	N/A	(39.20, −96.58)	Flask	*Lai et al.* [2006]	2001–2009	0.02, 0.38, 2.93	C_3/C_4grassland

Site Name (Manuscript Designation)	Network (AmeriFlux, NOAA, DOE-ARM Site Codes)	Location (Degrees Lat. Long.)	Sampling Frequency	Sampling Method	Years	Sampling Heights (m)	Vegetation
Salt Lake City	N/A	(40.76, −111.89)	Flask	*Pataki et al.* [2003a]	2005–2012	18	Urban
Southern Great Plains (SGP)	AmeriFlux (*US-ARM*); DOE-ARM (*SGP*)	(36.61, −97.49)	Flask	*Torn et al.*[2011]	2002–2012	2, 4, 9, 60	C_3/C_4grassland
Wind River	AmeriFlux *(US-Wrc)*	(45.82, −121.95)	Flask	*Lai et al.*[2005]	2001–2009	0.1, 10.2, 56	Temperate evergreen forest

- Continuous sampling frequency was every 30 min.
- a Flask collections from Niwot Ridge were taken at the tundra site (*NWR*) [*Dlugokencky et al.*, 2015; *White et al.*, 2015], including observations of CH_4 and CO used to diagnose anthropogenic contributions to the *US-NR1* forest site.

2.2 Site Sampling Protocol

The atmospheric CO_2 and $\delta^{13}C$ of CO_2 data collected at the sites (Figure 1) were part of separate past studies; therefore, the instrumentation, sampling heights, sampling frequency, and time frame varied (Table 2, Figure 1). Most vegetation sites (Harvard, Howland, Wind River, and Rannells) had discrete, multiheight flask sampling that followed the sampling protocol described by *Lai et al.* [2005]. At those sites, 55 day and 145 night samples were collected per year on average. Separate flask sampling protocols were used at *SGP* [*Torn et al.*, 2011], Salt Lake City [*Pataki et al.*, 2003a, 2007], and the tundra site at Niwot Ridge (*NWR*). *NWR* sampling was part of the long-term effort conducted by NOAA and the Stable Isotope Laboratory at the University

of Colorado [*Dlugokencky et al.*, 2015; *White et al.*, 2015] and is distinct from the forest site at Niwot Ridge (*US-NR1*). The *NWR* flask measurements were only used as a tool to identify periods of anthropogenic influence at *US-NR1* (section 2.6), but not to calculate δ_{source} at the site. Two sites also had continuous atmospheric $\delta^{13}C$ observations (half-hourly resolution), taken by a tunable diode laser absorption spectrometer at Niwot Ridge forest (*US-NR1*) [*Bowling et al.*, 2014] and by a quantum cascade laser spectrometer at Harvard Forest (growing season only) [*Wehr et al.*, 2013]. The sampling heights varied among the sites (Table 2) but included subcanopy, canopy, and above-canopy air at all the vegetated sites.

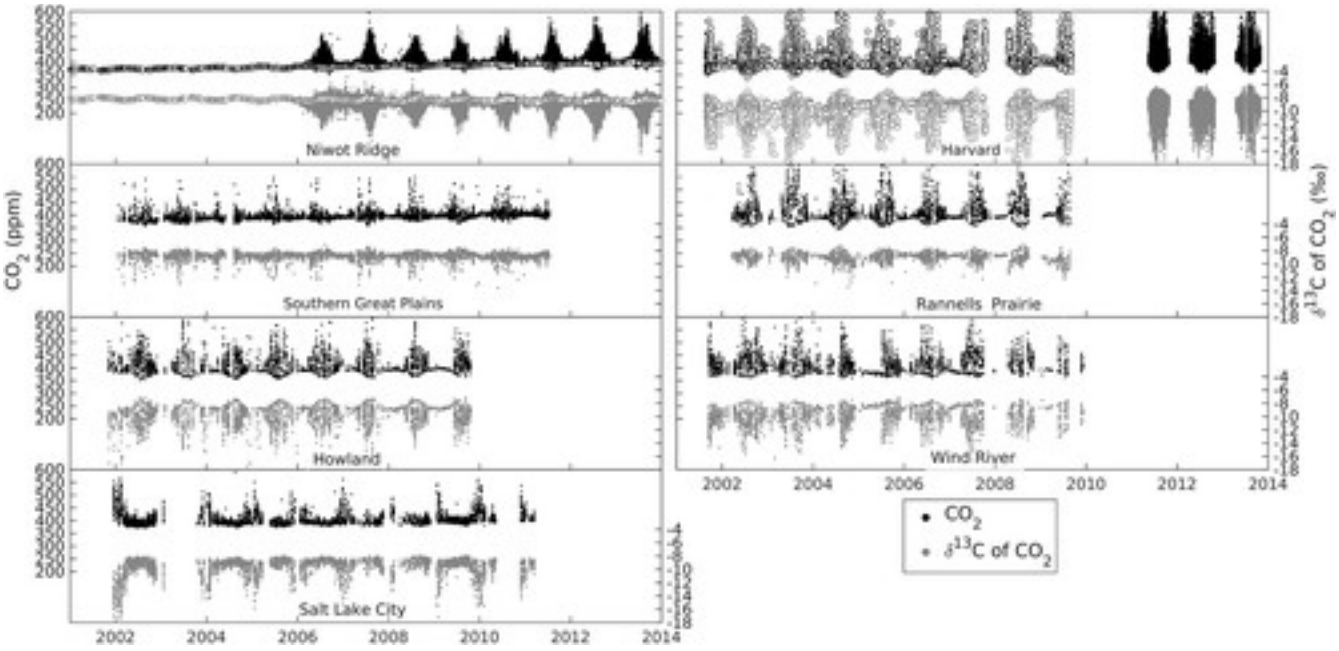

Figure 1

Open in figure viewerPowerPoint

Time series of atmospheric CO_2 (black symbols, left axes) and $\delta^{13}C$ of atmospheric CO_2 (gray symbols, right axes) for all sites. For Niwot Ridge and Harvard, the solid dots represent continuous, high-resolution observations whereas the open circles represent flask observations.

The atmospheric flask data of CO_2 and $\delta^{13}C$ of CO_2 for all sites is located within the Hydroshare repository [*Ehleringer*, 2017], with the exception of SGP (https://www.arm.gov/; DOI: 10.5439/1328127). The continuous data for Niwot Ridge (*US-NR1*) and Harvard are located at the Ameriflux website (http://ameriflux.lbl.gov/; DOI: 10.17190/AMF/1246088), and Harvard Forest Data Archive (http://harvardforest.fas.harvard.edu:8080/exist/apps/datasets/showData.html?id=hf209); respectively. The anthropogenic trace gas data for CH_4, CO, and CO_2 at the NWR tundra site is available at NOAA GMD (https://www.esrl.noaa.gov/gmd/dv/data/).

2.3 Calculating δ_{source}

We used a mixing model [*Miller and Tans*, 2003] with background correction [*Ballantyne et al.*, 2010] to calculate $\delta^{13}C$ of the local net land-atmosphere carbon exchange (δ_{source}). This approach assumes that the locally measured atmospheric CO_2 (C_a) is the combination of background CO_2 (C_{bg}) and local source CO_2 (C_{source}; which can be positive or negative based on whether there is a net emission or uptake of carbon to land) following conservation of mass:

$$C_a = C_{bg} + C_{source} \quad (1)$$

Similarly, the product of CO_2 and its isotopic composition (δ) is conserved [*Tans*, 1980], and following the conservation of mass of ^{13}C, the product of measured δ and CO_2 ($\delta_a C_a$) is the sum of the time varying background product ($\delta_{bg} C_{bg}$) and the local source product ($\delta_{source} C_{source}$) as

$$\delta_a C_a = \delta_{bg} C_{bg} + \delta_{source} C_{source} \quad (2)$$

Rearranging equations 1 and 2 yields the Miller-Tans relationship, with a variable background specified [*Ballantyne et al.*, 2010] as

$$\delta_a C_a - \delta_{bg} C_{bg} = \delta_{source} \left(C_a - C_{bg} \right) \quad (3)$$

The δ_{source} value was calculated by linear regression of $\delta_a C_a - \delta_{bg} C_{bg}$ against $C_a - C_{bg}$. A major advantage of this approach is that the δ_{source} signal is isolated from time-varying changes in the background atmospheric composition, allowing one to distinguish local changes from regional changes.

An established approach [e.g., *Ballantyne et al.*, 2010] to specify the background terms within equation 3 is to fit a function to a set of discrete observations and use that fitted function to account for shifts in background mole fraction (illustrated in Figure 2). We refer to this variant as the *smoothed* approach where $C_{smoothbg}$ and $\delta_{smoothbg}$ are interpolated from a smoothed background function as defined as

$$\delta_a C_a - \delta_{smoothbg} C_{smoothbg} = \delta_{smoothsource} \left(C_a - C_{smoothbg} \right) \quad (4)$$

We used a curve-fitting technique to create the background function required for equation 4that is provided by NOAA (http://www.esrl.noaa.gov/gmd/ccgg/mbl/crvfit/crvfit.html) which is based on a harmonic curve fitting method [*Thoning et al.*, 1989] with an 80 day short-term cutoff filter. We fit curves independently to the discrete observations from the tallest inlet height (Figure 2) to create $C_{smoothbg}$ and $\delta_{smoothbg}$ for each site. To resolve the seasonal change in δ_{source}, we applied the regression in a 3 month window of data (centered in each of 12 months) grouped across all years (Figure 3), as in *Ballantyne et al.* [2010]. This approach maximized the number of samples for the regressions. This provided a more stable and consistent seasonal cycle as compared to using only a 1 month moving window. First, we performed the regression on a 3 month moving

window for all the observations and created a preliminary δ_{source}. Next, we calculated the residuals between the preliminary regression and the observations. We then filtered the data by removing observations that most poorly fit the preliminary regression—those with residuals greater than the 95th percentile were removed (Figure 3, in gray). The filtering step removed outliers that could have a large impact on the regression slope. Next, we performed the regression on the remaining data to calculate the final δ_{source} (Figure 3, in black). We used Model 1 ordinary least squares regression [*Zobitz et al.*, 2006]. We considered regressions with an $R^2 < 0.90$ a poor fit, and these were not used in our analysis.

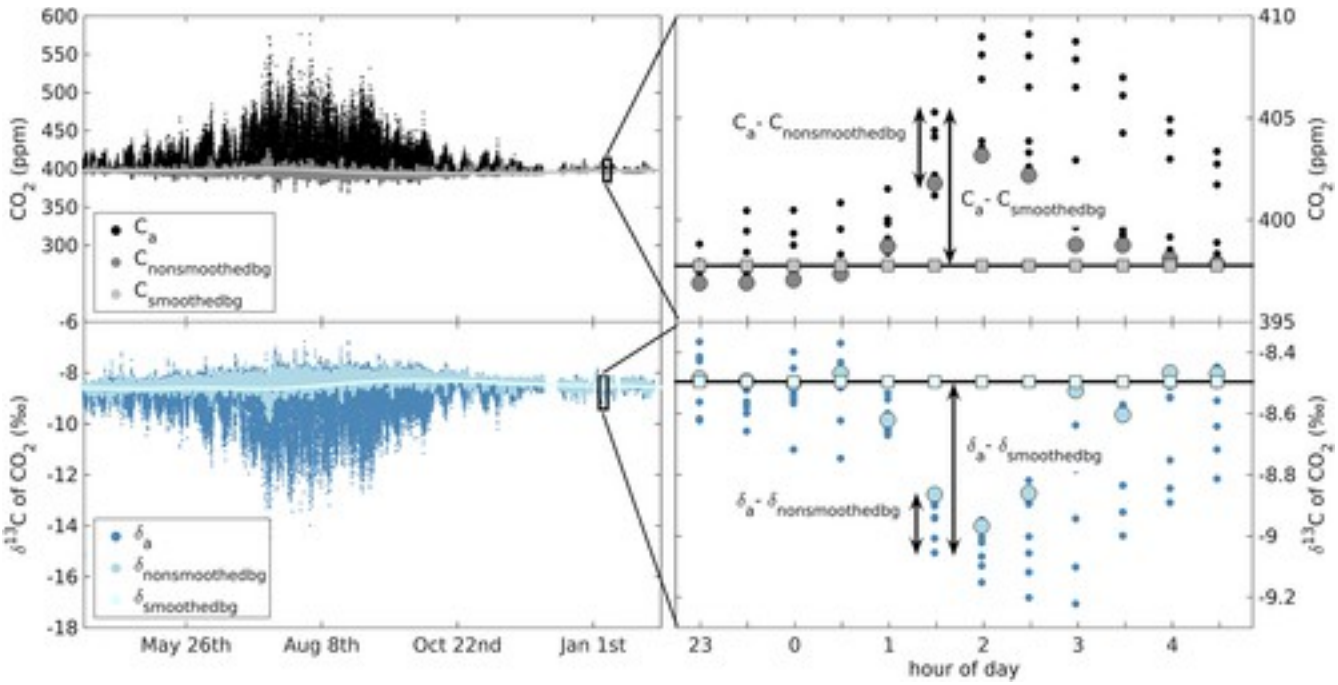

Figure 2

Open in figure viewerPowerPoint

Step 1 of our approach for calculating the δ_{source} using *US-NR1* as an example. The data at all tower heights (black CO_2; dark blue $\delta^{13}C$) are adjusted by the *nonsmoothed* background data (medium gray CO_2; medium blue $\delta^{13}C$) for the *nonsmoothed* approach or adjusted by the harmonic fit of the background data (light gray CO_2; light blue $\delta^{13}C$) for the *smoothed*approach. The figure insets (top right: CO_2, bottom right: $\delta^{13}C$) are zoomed-in to illustrate the difference in approaches.

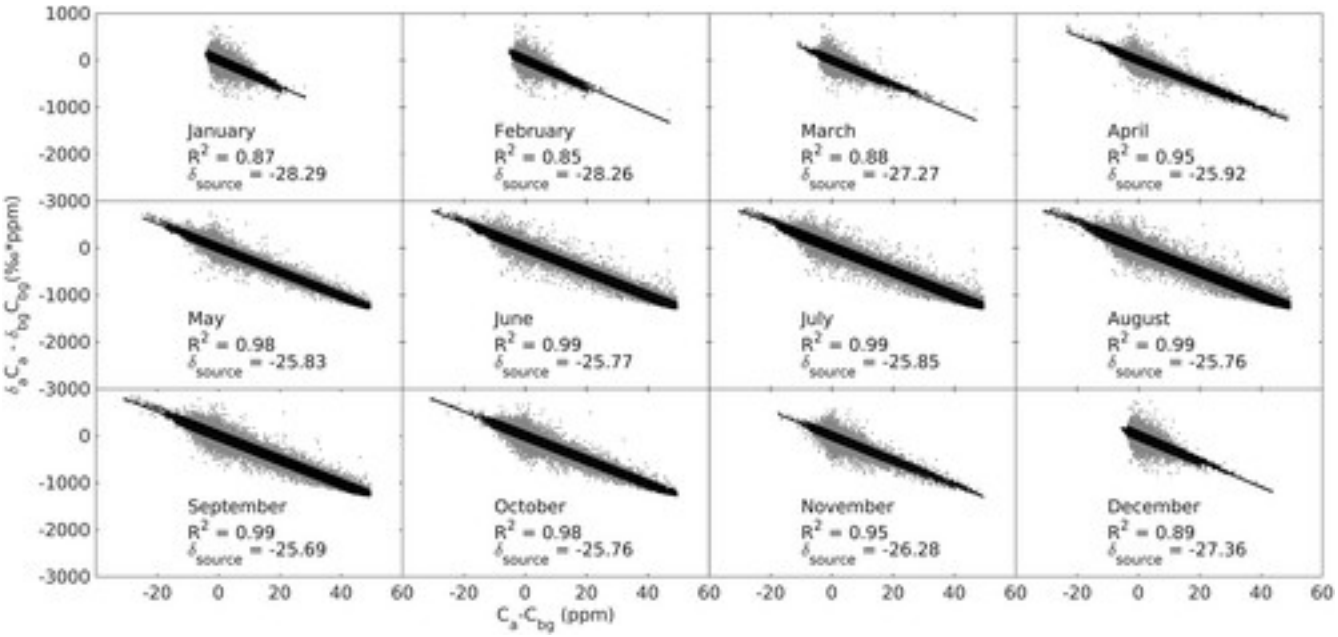

Figure 3

Open in figure viewerPowerPoint

Step 2 of our approach used linear regressions between $C_a - C_{bg}$ and $\delta_a C_a - \delta_{bg} C_{bg}$ (from Figure 2). The slopes of the linear regressions provide the δ_{source}. The gray dots represent all data available in each time window (Figure 2), whereas the black dots represent data after outlier removal as described in the text. Shown here are results from the 3 month *smoothed*Miller-Tans approach where the data were adjusted with the interpolated harmonic fit and aggregated into a 3 month moving window (centered on the indicated months) across all years for each panel. The R^2 and δ_{source} shown were calculated from the data with outliers removed.

Second, we used a variation of the above approach to account for shifts in background by utilizing concurrent (in time) background and local site observations without curve fitting (e.g., *US-NR1*; Figure 2 and Figures S1 and S2 in the supporting information). We refer to this method as the *nonsmoothed* approach where the *nonsmoothed* background CO_2($C_{nonsmoothbg}$) and $\delta^{13}C$ ($\delta_{nonsmoothbg}$) were directly measured from the tallest inlet height at each site and defined similarly to equation 4. The advantage of the *nonsmoothed* approach is that it accounts for high-frequency, short-duration changes in background mole fraction and isotope composition that are missed by the *smoothed* approach. In this analysis, however, only *US-NR1* and *SGP* had sufficient data to perform the *nonsmoothed* approach in which to quantify the difference in δ_{source} between methods (section 2.6). The δ_{source} was calculated using the *nonsmoothed* approach identically to the *smoothed* approach as described in section 2.3 (Figures S1 and S2). Similar plots to Figures S1 and S2 were created for *SGP* for the *smoothed* approach (Figure S3), *nonsmoothed* approach (Figure S4), and regression statistics (Figure S5) and are included in the supporting information.

2.4 Calculating the Site-Level ^{13}C Isoforcing

We calculated the site-level isoforcing to quantify and compare the impact of net land-atmosphere exchange of $^{13}CO_2$ of different land surface types upon δ_{atm}. Following *Lee et al.* [2009], isoforcing is defined as

$$\text{isoforcing} = \frac{\text{NEE}}{C_{av}}\left(\delta_{\text{smoothsource}} - \delta_{\text{atm}}\right). \quad (5)$$

For AmeriFlux sites, we calculated monthly average isoforcing with the monthly average NEE calculated from L4 or L2 data (http://ameriflux.lbl.gov/; DOIs—Niwot Ridge: 10.17190/AMF/1246088, Harvard: 10.17190/AMF/1246059, Howland: 10.17190/AMF/1246061, Konza: 10.17190/AMF/1246068, SGP: 10.17190/AMF/1246027) and the monthly $\delta_{smoothsource}$ (equation 4), with the exception of *US-Wrc* where we used NEE provided directly from the site PI [*Wharton et al.*, 2012]. The carbon balance at Salt Lake City is primarily controlled by anthropogenic emissions [*Strong et al.*, 2011]; therefore, we calculated the isoforcing from anthropogenic emissions of natural gas, petroleum, and coal for 2014 within Salt Lake County (Hestia model [*Patarasuk et al.*, 2016], provided by Daniel Mendoza and included in the supporting information) combined with the $\delta^{13}C$ of combustion of petroleum [*Bush et al.*, 2007], natural gas [*Pataki et al.*, 2003a, 2007], and coal. To provide a consistent comparison of isoforcing across sites, we used observations from *NWR* to define the atmospheric concentration of CO_2 (C_{av}) and δ_{atm}. The same data years were used for each site to obtain site-level NEE (AmeriFlux) and $\delta_{smoothsource}$ (Table 2) to calculate the isoforcing (equation 5) with the exception of Salt Lake City.

Cropland such as corn and soybean were not explicitly included in our analysis, yet they significantly impact the regional carbon (and ^{13}C) budget within the United States as estimated by land surface models [*Huntzinger et al.*, 2012] and atmospheric inversions [e.g., *Lauvaux et al.*, 2012]. Considering the importance of these cropland species in influencing the carbon budget, we estimated the isoforcing of corn and soybean sites (Figure S6) through carbon uptake [*Lokupitiya et al.*, 2009] and δ_{photo} values for these species [*Dercon et al.*, 2006].

2.5 Diagnosing the Impact of VPD on δ_{source}

We calculated the correlation between monthly VPD and monthly δ_{source} (section 2.3) to identify if δ_{photo} drives seasonal changes in δ_{source} through stomatal conductance responding to VPD. We calculated a monthly average VPD from the daytime site-level VPD data obtained from AmeriFlux (http://ameriflux.lbl.gov/; same site DOIs as section 2.4). We tested for correlation with the Pearson correlation coefficient (r) and determined significance when $p < 0.05$.

2.6 Diagnosing the Impact of Anthropogenic Trace Gases on δ_{source}

A previous analysis at *US-NR1* found that the sporadic influence of anthropogenic gases on local atmospheric measurements, particularly during winter, may have led to an erroneously high seasonal amplitude of δ_{source} [*Bowling et al.*, 2014]. This finding was reached because the relatively depleted winter δ_{source} using the *smoothed* approach could not have resulted from the influence of biogenic sources alone. Here we diagnosed to what extent the *smooth*and *nonsmoothed* approaches removed the background anthropogenic influence from the local δ_{source}. First, we leveraged a wide range of flask measurements at *NWR* that have been analyzed for CH_4 and CO—both trace gases that indicate anthropogenic influence. We identified periods of anthropogenic influence at *NWR* when mole fractions of CH_4 and CO were anomalously high as compared to their background values. These anomalies were calculated as the difference between the discrete flask measurement taken at the tundra site at Niwot Ridge and a harmonic fit [*Thoning et al.*, 1989] to the flask time series. As shown later, sporadic anthropogenic anomalies of CH_4 and CO during the winter were strongly linked to CO_2 anomalies, and we assumed that these events also affected nearby Niwot Ridge forest (*US-NR1*).

3 Results

3.1 Seasonality of Smoothed δ_{source}

The average annual δ_{source} for a 3 month moving window was the most enriched for grassland sites (−19.0 ± 4.4‰ across-year standard deviation), most depleted for the urban site (−29.7 ± 2.2‰), and the forested sites were in between (−27.0 ± 1.5‰). Within the forested sites, the δ_{source} of conifer stands (−26.8 ± 1.1‰) was indistinguishable from the deciduous stand (−26.5 ± 0.2‰; Figure 4). The annual averages of δ_{source} for the 1 and 3 month moving windows were similar; however, there was more variability for the 1 month δ_{source}. The seasonal amplitudes of δ_{source} for the 3-month moving window were largest for Salt Lake City and *SGP* (5.9‰ and 4.7‰, respectively), whereas the seasonal amplitude was smallest for the forested sites (excluding Harvard) with average amplitude of 4.1‰ (Figure 4).

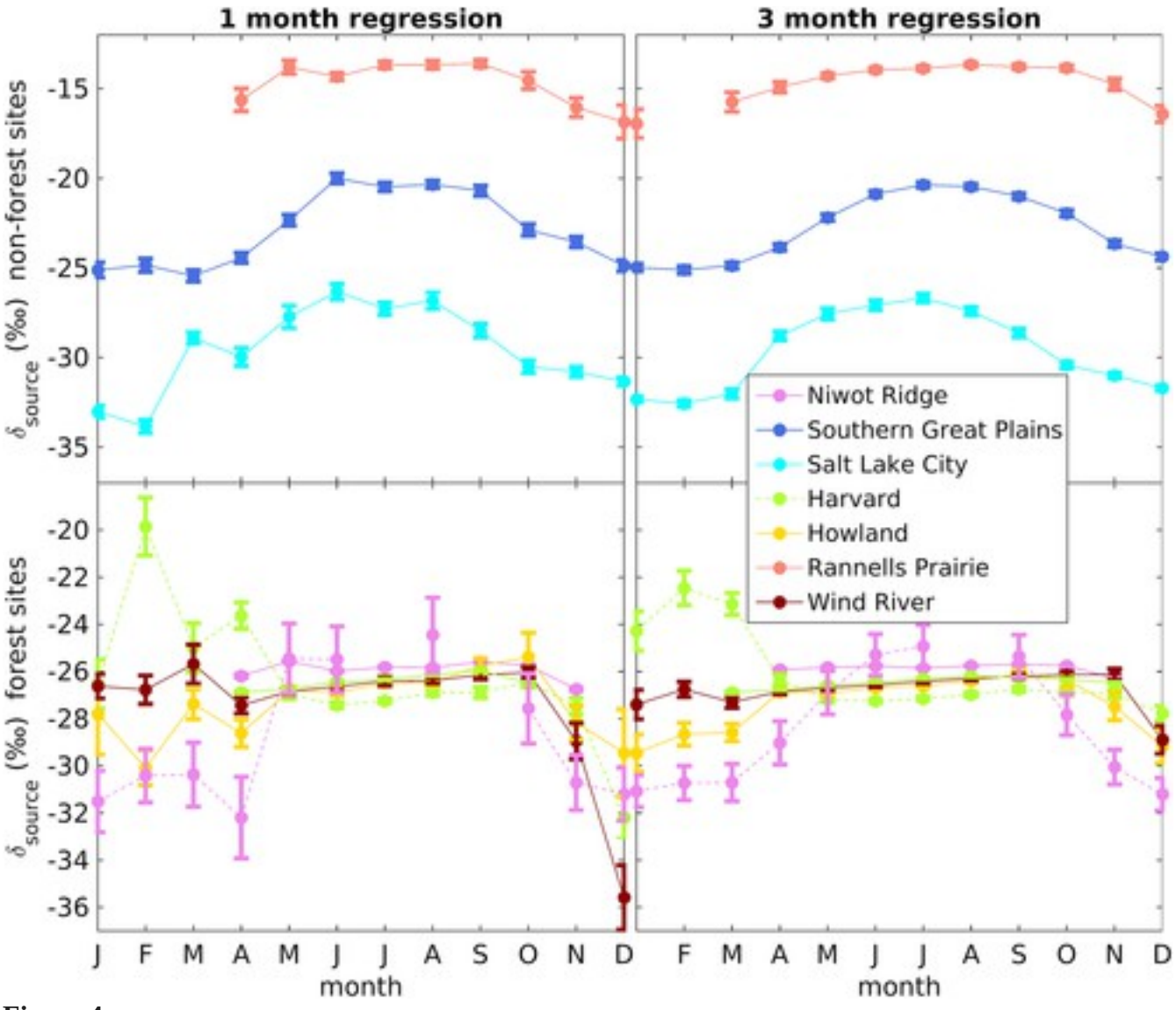

Figure 4

Open in figure viewerPowerPoint

An across-site comparison of seasonality of δ_{source} using the s*moothed* approach. For Niwot Ridge and Harvard, the solid and dashed lines were based on continuous and flask observations, respectively. (top) Results from the grassland and urban sites (*SGP*, Salt Lake City and Rannells) and (bottom) from the forest sites only. The uncertainty bars are the 95% confidence intervals for the regression fits and are smaller than the symbols in some cases.

3.2 Impact of *Smoothed* Versus *Nonsmoothed* Background on δ_{source}

The choice of background method had no significant impact upon the seasonal amplitude of δ_{source} for *SGP*, but the peak in δ_{source} shifted 1 month later for the nonsmoothed approach. The seasonal variation of δ_{source} for *US-NR1*, however, was eliminated with the *nonsmoothed*approach

(Figure 5). The seasonal amplitude in δ_{source} remained about the same for *SGP*whether using the *smooth* or *nonsmoothed* approach as the amplitudes were 4.7‰ and 5.0‰, respectively. The *US-NR1* δ_{source}, on the other hand, reduced from a seasonal amplitude of 2.6‰ to 0.6‰ from the smoothed to nonsmoothed approach, respectively (Figure 5).

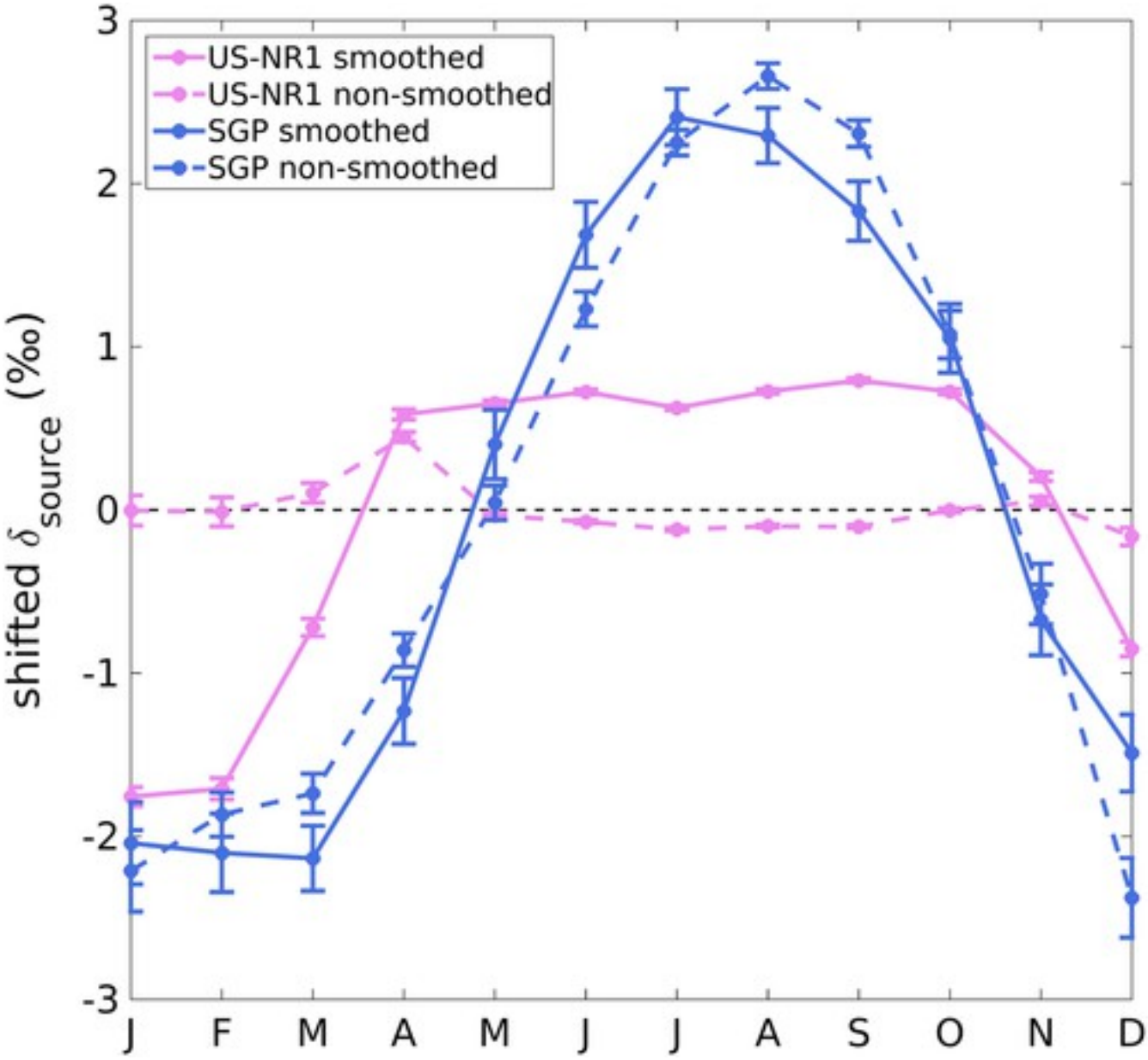

Figure 5

Open in figure viewerPowerPoint

The impact of both approaches on the mean seasonal pattern of δ_{source} between *US-NR1* and Southern Great Plains (*SGP*). The annual mean δ_{source} was subtracted for each site/method for improved comparison of their seasonal pattern.

3.3 Impact of Anthropogenic Trace Gases at Niwot Ridge on δ_{source}

High CO_2 events (C_a) at the *NWR* in winter were often associated with large contributions of anthropogenic trace gases. Flask observations revealed strong correlations between anomalies of CO_2 and anomalies of anthropogenic trace gases with R^2 values of 0.72 and 0.51 for CH_4 and CO, respectively (Figure 6). This finding suggests that the highest CO_2anomalies at the nearby Niwot Ridge forest site (*US-NR1*) were also related to anthropogenic influence given the two sites are less than ~5 km apart. Therefore, we examined the highest CO_2 anomaly data periods at *US-NR1* to diagnose the impact of anthropogenic influence upon δ_{source} for *US-NR1* only.

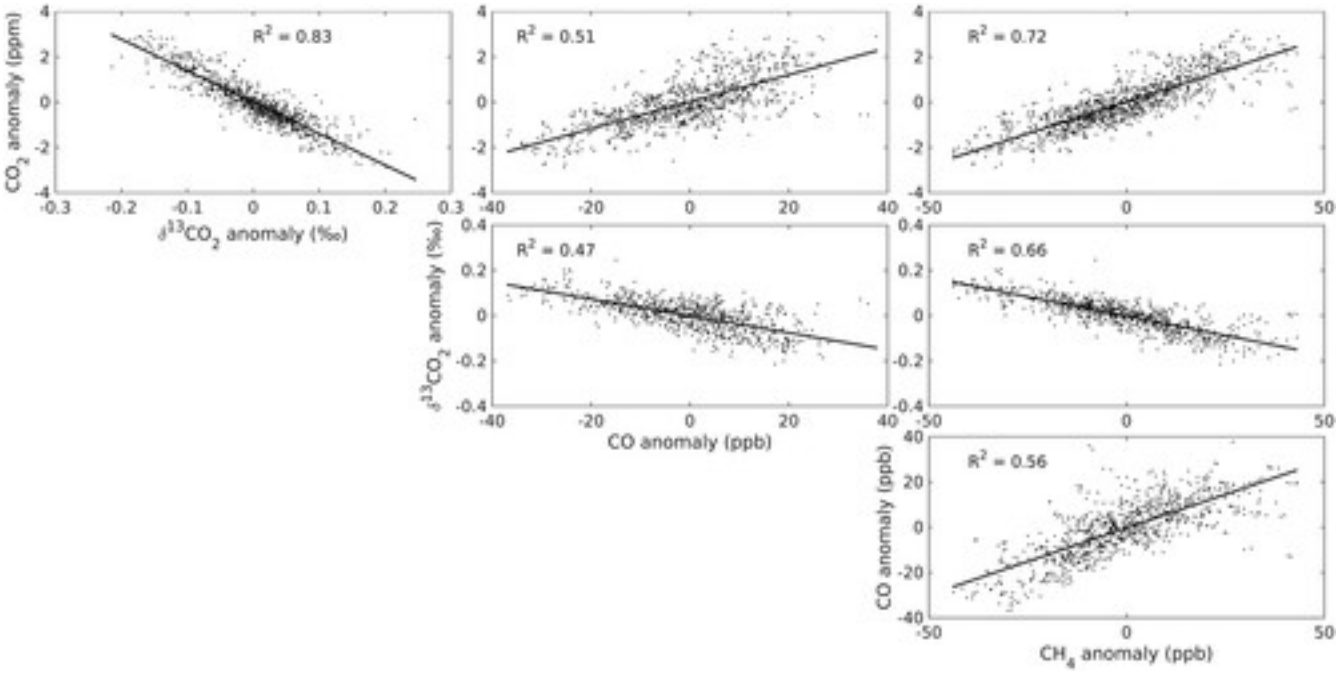

Figure 6
Open in figure viewerPowerPoint
A demonstration of anthropogenic trace gases at Niwot Ridge that likely impacted the *smoothed* analysis during the winter. The data are from the winter (November–March) flask observations for the Niwot Ridge tundra site (*NWR*). The anomalies of CO_2, $\delta^{13}C$, CH_4, and CO are the residuals between the raw data and the harmonic fit of the raw data.

Time periods associated with the highest CO_2 anomaly events at *US-NR1* led to lower (more negative) δ_{source} when calculated with the *smoothed* approach, but not for the *nonsmoothed*approach where δ_{source} was more enriched and nearly identical regardless of time period (Figure 7). The δ_{source} from December through February calculated with the *smoothed*approach had a monthly average of −28.8 ± 1.5‰ and −28.2 ± 1.1‰ for the highest (>95% and >90%) CO_2 anomalies, respectively, and −27.2 ± 0.4‰ and −27.2 ± 0.4‰ for when these anomalous periods were removed. Likewise, the December through February annual

averages of δ_{source} calculated with the *nonsmoothed* approach were −25.5 ± 0.2‰ and −25.6 ± 0.2‰ for only the highest >95% and >90% CO_2 anomalies and −25.8 ± 0.1‰ and −25.7 ± 0.2‰ when these periods were removed.

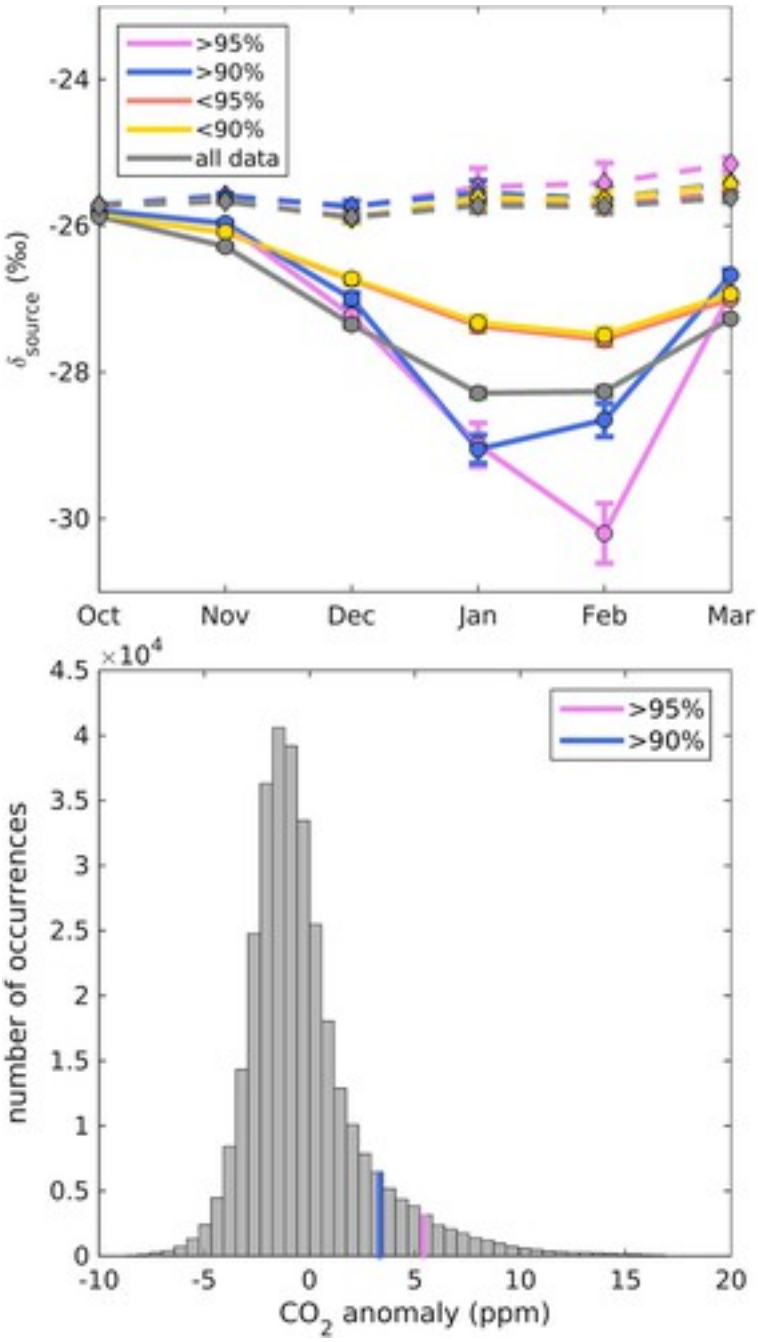

Figure 7

Open in figure viewerPowerPoint

(top) The winter season δ_{source} plotted by percentiles of the largest CO_2 anomalies (based on harmonic fit) for all sample heights for *US-NR1*. The δ_{source} was calculated from the CO_2 and $\delta^{13}C$ continuous observations corresponding to the time periods of highest CO_2 anomalies (>95% or

>90%) or for the remaining data with anomalies removed (<95% or <90%), respectively. The solid and dashed lines represent the *smoothed* and *nonsmoothed*approaches (3 month aggregation) for calculating δ_{source}, respectively. (bottom) Histogram of the CO_2 anomalies, with vertical lines of the 95th and 90th percentiles, respectively.

3.4 Influence of VPD on Seasonality of δ_{source}

There were no significant correlations between the growing season (April–September) monthly mean values of δ_{source} and VPD, with the exception of Wind River and *SGP*(Figure 8). Three out of four forested sites showed no correlation between δ_{source} and VPD (forest average r = 0.15), whereas the grassland sites of *SGP* and Rannells were more highly correlated (average r = 0.82). VPD values increased at each site from spring (April–June) through peak summer (July), followed by a decrease in late summer (August–September). On the other hand, the monthly δ_{source} for all sites but Harvard increased slightly during this period (April–September) on average of 1.1‰.

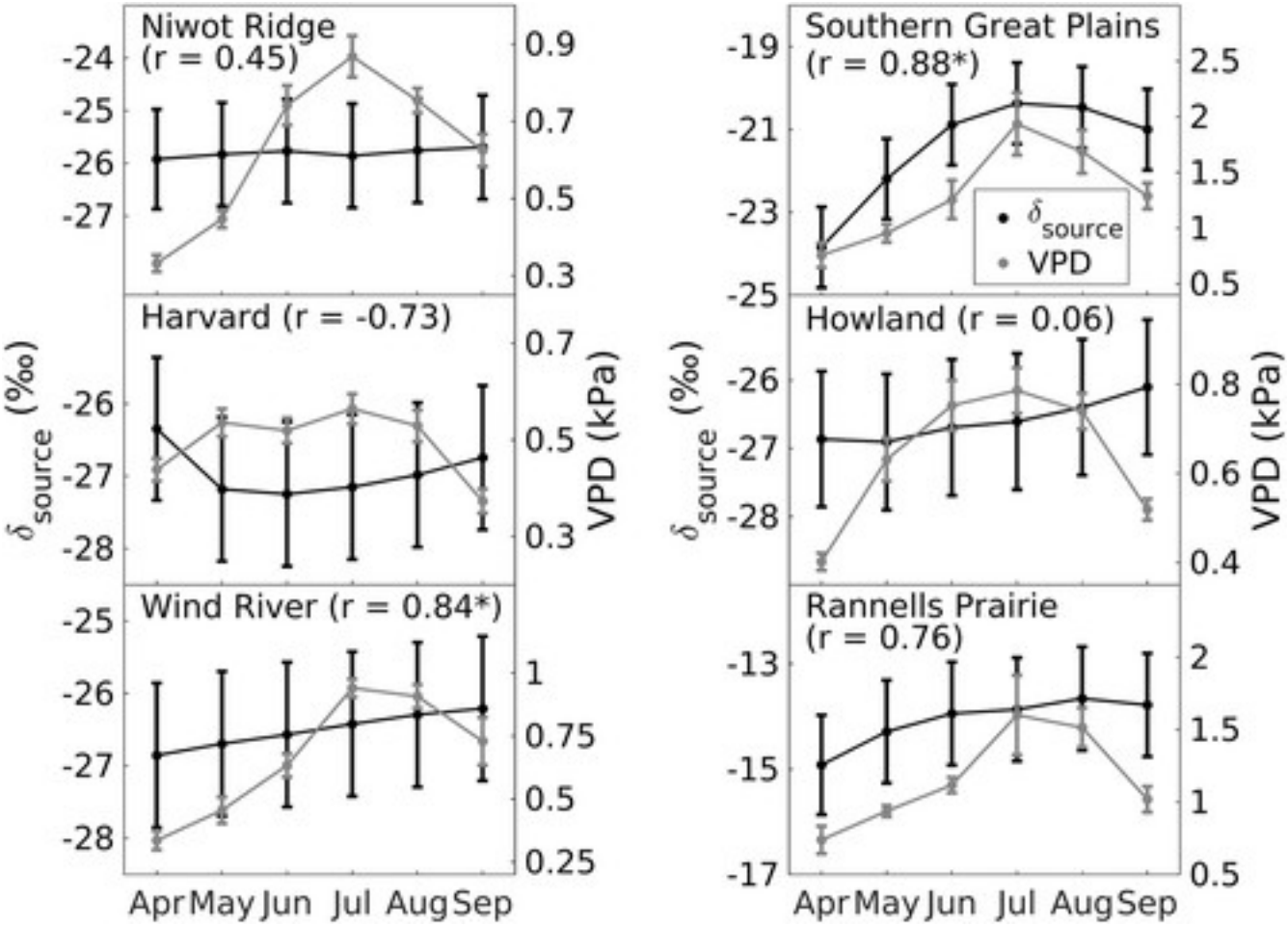

Figure 8
Open in figure viewerPowerPoint

The monthly average δ_{source} (left axes) as calculated by the *smoothed* approach (3 month window; Figure 4) superimposed on monthly mean VPD (right axes). The uncertainty bars for δ_{source} are the 95% confidence interval for the regression fits, and the uncertainty bars for the VPD are the standard error of the interannual variation. Each panel includes the Pearson correlation coefficient (r) between the monthly VPD and δ_{source}, where * indicates a significant correlation (p value < 0.05).

3.5 Impact of Land Surface Type on δ_{atm}

The isoforcing is an indicator of the influence of land cover type on δ_{atm}. Harvard Forest had the largest positive ^{13}C isoforcing (making δ_{atm} more enriched from net carbon uptake by photosynthesis), whereas Salt Lake City had the most negative ^{13}C isoforcing (making δ_{atm}more depleted from net release of carbon from fossil fuel combustion) with annual averages of $+1.0 \times 10^{-3}$ and -7.0×10^{-3}‰ μmol m s^{-1}, respectively (Figure 9). Similar to Harvard Forest, the conifer forest and grassland sites also showed positive but smaller annual average isoforcing of 0.5×10^{-3} and 0.3×10^{-3}‰ μmol m s^{-1} respectively. Whereas a negative isoforcing persisted in Salt Lake City throughout the year, the sites dominated by vegetation switched sign in isoforcing during the year reflecting the change in sign in NEE (carbon sink summer, carbon source winter).

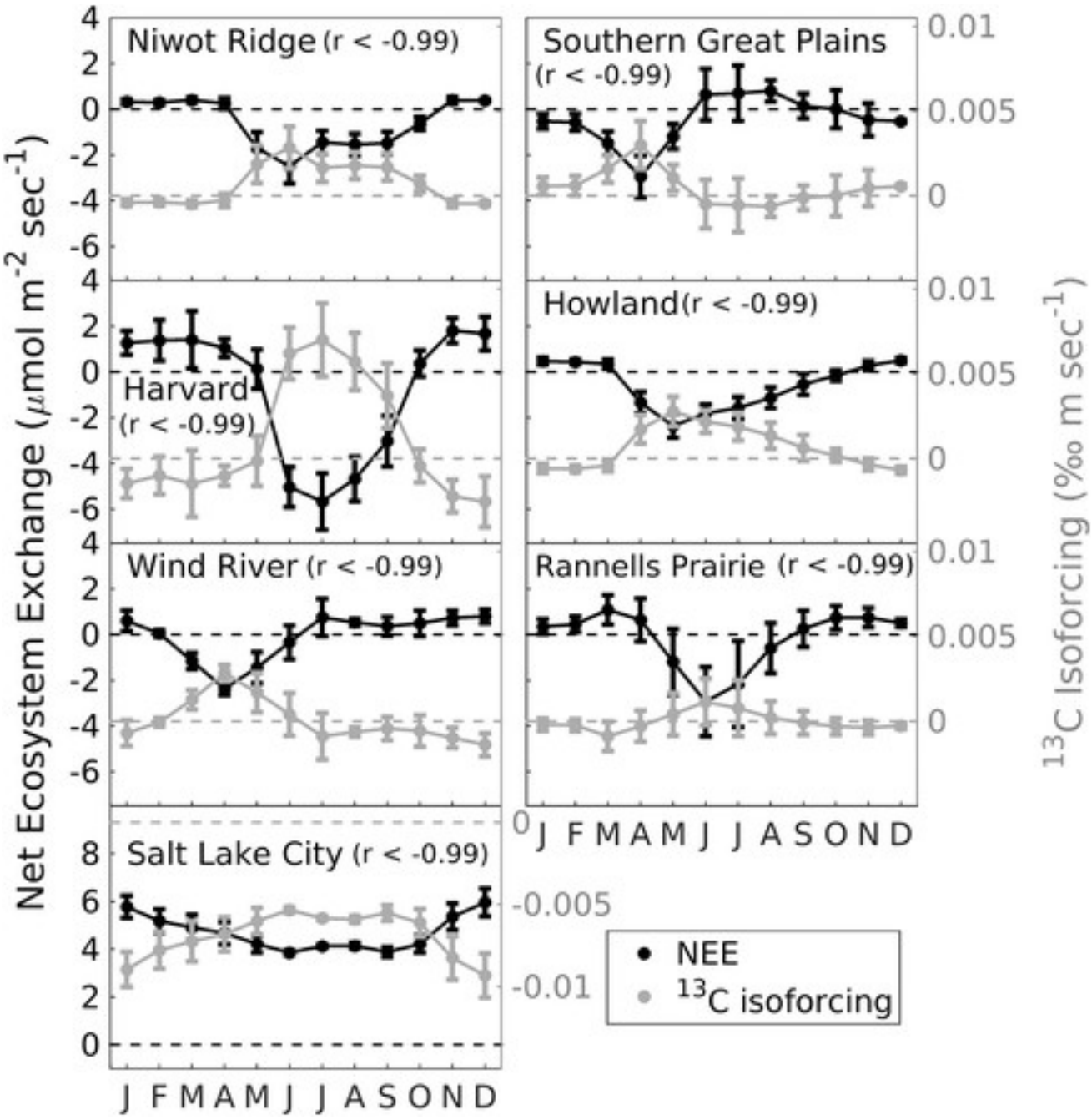

Figure 9

Open in figure viewerPowerPoint

The seasonality of monthly mean NEE (black) and isoforcing (gray) for each site. The isoforcing values (equation 5) were calculated using the monthly average NEE and the monthly average δ_{source} values as determined by the *smoothed* approach (except SLC which used Hestia emissions for NEE and literature values of fossil fuel for $\delta^{13}C$). The uncertainty bars are based on the 1σ interannual variation for the monthly NEE and 1σ uncertainty for the monthly isoforcing value.

The deciduous Harvard Forest imparted the largest seasonal peak-to-peak magnitude of isoforcing (9.6×10^{-3}‰ μmol m s^{-1}), and all other sites averaged a smaller seasonal change

(3.3×10^{-3}‰ µmol m s^{-1}). Although Salt Lake City imparted the largest absolute value of isoforcing overall, the seasonal change was similar to most of the nonurban-dominated sites at 4.0×10^{-3}‰ µmol m s^{-1}. The timing of peak isoforcing varied between sites with Wind River and the *SGP* peaking the earliest (April), followed by Howland (May), *US-NR1* and Rannells (June), and finally Harvard (July). Among all sites, the peak isoforcing at Harvard Forest coincided most closely with the seasonal peak of δ_{atm} at *NWR* (Figure S6). Specifically, the seasonal pattern of the Harvard Forest isoforcing preceded the seasonal pattern of the troposphere at this latitude (δ_{atm} at *NWR*) by 1–2 months throughout the year.

The main driver of seasonal variation in ^{13}C isoforcing for all sites was the NEE, which is dominated by fossil fuel emissions in Salt Lake City. This is demonstrated by the strong anticorrelation between monthly NEE and isoforcing for each site based on the Pearson correlation coefficient (Figure 9). The seasonal variation in δ_{source} played only a minor role in influencing the seasonal isoforcing (Figure 4).

4 Discussion

4.1 Impact of VPD on Seasonal δ_{source}

Using the Miller-Tans mixing model and atmospheric observations of CO_2 and δ_{atm}, we detected a seasonal pattern in δ_{source} for all sites; however, this seasonal pattern was not driven by VPD. We arrive at this conclusion based both on the overall lack of strong correlation between seasonal changes in VPD and in δ_{source} and on the inconsistent relationship between VPD and δ_{source} across sites (Figure 8; section 3.4). Atmospheric water vapor can influence leaf stomatal conductance [*Farquhar et al.*, 1982], thereby reducing the ratio of leaf intracellular to atmospheric CO_2 that subsequently reduces the magnitude of photosynthetic discrimination [*Brugnoli et al.*, 1988; *Farquhar et al.*, 1989]. Given this physiological relationship, it is possible for VPD to correlate with the magnitude of photosynthetic discrimination and δ_{source}; however, we found no evidence of this for three of the four forested sites in this analysis (Figure 8). There are several explanations for why there was not a seasonal relationship between VPD and δ_{source}. First, although environmental variables such as VPD, T_{air}, and PAR are known to impact δ_{photo} [*Farquhar et al.*, 1982; *Alstad et al.*, 2007], this signal may not propagate to δ_{source} given that it is a combination of isotopic signals from both photosynthesis and ecosystem respiration—the respiration flux itself comprising a relatively fast response autotrophic and slow response heterotrophic contributions [*Bowling et al.*, 2008; *Brüggemann et al.*, 2011]. Second, seasonal variation in soil moisture, VPD, and photosynthetic capacity (influenced by air temperature and PAR) can covary and make it difficult to disentangle the effects. The lack of

correlation between VPD and δ_{source} is consistent with a modeling study [*Raczka et al.*, 2016] performed at *US-NR1* that demonstrates that VPD does not have a major influence upon photosynthetic discrimination on seasonal timescales at that location. There was a significant correlation between VPD and δ_{source} at Wind River, but part of this correlation was likely from soil moisture stress during summer. Wind River experiences an exceptionally strong seasonal gradient in precipitation with only 5% falling during June, July, and August [*Shaw et al.*, 2004]. Previous studies at Wind River have demonstrated that soil moisture content is correlated with δ_{resp} [*Lai et al.*, 2005] and that soil moisture stress, in addition to VPD, impacts the stomatal conductance [*Wharton et al.*, 2009; *Duarte et al.*, 2016] and thus δ_{source}. Furthermore, the old growth forest at Wind River (450–500 years old) has a stronger reduction in canopy conductance as compared to younger trees near the same location in response to dry conditions [*Fessenden and Ehleringer*, 2002; *Wharton et al.*, 2009]. This increased response by old growth forest to dry conditions is attributed to hydraulic constraints on stomata due to stand-age effects [*Ryan and Yoder*, 1997; *Woodruff et al.*, 2007] which contribute to the difference in correlation between VPD and δ_{source} at *US-Wrc*, compared to younger forests (*US-NR1*, Howland, Harvard).

At the grassland sites, VPD and δ_{source} were highly correlated (Figure 8); however, the correlation is likely unrelated to the physiological influence of VPD on stomatal conductance. The variation of seasonal productivity of C_3 and C_4 grasses has been attributed to optimum photosynthetic temperature [e.g., *Kemp and Williams*, 1980] and water availability [e.g., *Paruelo and Lauenroth*, 1996]. C_4 grasses discriminate much less against ^{13}C as compared to C_3 grasses, and this can lead to the seasonal rise and fall of δ_{source} as demonstrated by a C_3/C_4 end member mixing model at *SGP* [*Torn et al.*, 2011] and other grassland sites [*Lai et al.*, 2003; *Still et al.*, 2003b]. Other factors besides the relative contribution of C_3/C_4productivity may have contributed to the seasonal variation in δ_{source}. For example, the change in seasonal VPD likely impacted the stomatal conductance and photosynthetic discrimination of the C_3 grasses, although the impact of stomatal conductance on seasonal discrimination is known to be small (1–2‰) [*Mole et al.*, 1994; *Still et al.*, 2003b]. In addition the observation tower height at *SGP* (60 m) led to a large vegetation "footprint" capable of influencing the tower observations. It is likely the atmospheric measurements at the tower were influenced by cropland (primarily winter wheat) outside of the immediate mixed C_3/C_4natural grass area. The influence of winter wheat (C_3 photosynthesis) at SGP is consistent with a δ_{source} that is 5‰ more depleted than Rannells Prairie (Figure 4). The relatively large size of the vegetation footprint combined with a possible seasonal shift in area and extent of the footprint may have played a role in the seasonal δ_{source} [*Griffis et al.*, 2010; *Torn et al.*, 2011]. Nevertheless, the similarity of the seasonal pattern in δ_{source} found at the Rannells

grassland site (Figure 4), which has a smaller footprint than *SGP* (~3 m height), suggests that the effect of a shifting footprint at *SGP* was relatively small.

4.2 Drivers of Seasonal Amplitude of δ_{source} and Isoforcing

The largest seasonal amplitudes in δ_{source} were found at the grassland and urban sites, driven by the transition in productivity between C_3 and C_4 grasses and the intensity and timing of fossil fuel emissions, respectively. This finding is consistent with separate analyses at *SGP* [*Torn et al.*, 2011] and at Salt Lake City [*Pataki et al.*, 2003a]. Similar flask data were analyzed by different methods for *SGP* between this analysis (2002–2012) and *Torn et al.*[2011] (2002–2010). *Torn et al.* used the Keeling plot approach [*Pataki et al.*, 2003b], subset the flask data into day and night, and grouped the data by months from separate years. This analysis, however, used the *smoothed* and *nonsmoothed* approaches and grouped all the data into a single seasonal cycle. Regardless of the regression approach and flask data grouping between these separate analyses, the seasonal δ_{source} ranged from −25‰ during the winter to −20‰ during the summer (Figures 4 and 5). The consistency in the pattern and amplitude in δ_{source} is an indication that the background δ_{source} or CO_2 mole fraction does not change significantly at *SGP* within the months that the regression is performed. A relatively constant background signal within a single month seems feasible, given the seasonal atmospheric change of δ_{atm} in the Northern Hemisphere is <0.4‰ (Figure S6).

The seasonal change of δ_{source} at Salt Lake City ranged from −35‰ in the winter to −28‰ in the summer for 2002 [*Pataki et al.*, 2003a] and −33‰ to −27‰ (2005–2012) for this analysis. The δ_{source} seasonal amplitude was nearly identical despite the differences in the methods: the Keeling plot [*Pataki et al.*, 2003a] and *smoothed* approach (this analysis). The similarity of the δ_{source} seasonal cycle between 2002 and 2005–2012 suggests that the timing and contribution of emissions in Salt Lake City were similar with a higher proportion of natural gas emissions during the winter for home heating (−37.7‰) and a higher proportion of gasoline combustion (−28.3‰) during the summer [*Bush et al.*, 2007]. These seasonal ranges of values found for Salt Lake City were similar but more depleted than those calculated in the urban area of Heidelberg, Germany (summer: −25.0‰, winter: −32.5‰) [*Vardag et al.*, 2016]. In general, the seasonal pattern and amplitude of δ_{source} at Salt Lake City reflect the dominance of natural gas combustion for heating in winter and transportation in summer [*Pataki et al.*, 2003a]. Whether this seasonal pattern applies to other urban areas depends upon the dominant local energy sources (natural gas versus petroleum, wood, coal, heating oil, etc.) and their seasonal demands.

Compared to previous analyses, we found relatively small seasonal variation in δ_{source} at the forest sites. The average seasonal amplitude of δ_{source} for forest sites found here (2.3‰) is smaller than forest sites determined by similar methods including a conifer forest in North Carolina (3.7‰) [*Ballantyne et al.*, 2010] and the average of five midlatitude forest sites within the United States and Europe (3.7‰) [*Ballantyne et al.*, 2011]. The methods employed by *Ballantyne et al*. and in our analysis are identical with the important exception of the proximity of the background location to the site observations. *Ballantyne et al.* chose a remote, upwind, high-altitude alpine tundra site (*NWR*) to remove regional land and anthropogenic influences. We, on the other hand, used a background nearly collocated with the site itself, which isolated the influence on δ_{source} to the region immediately surrounding the site (~1–10 km^2). Therefore, the difference in δ_{source} between the remote [*Ballantyne et al.*, 2010] and near (our analysis) background corrections likely results from the difference in land "footprint." Our analysis suggests that when the local forest signal is isolated to the area within the tower footprint, the seasonal change in growing season δ_{source} is relatively small, whereas using a remote background will include upwind fluxes from both ecosystem and anthropogenic sources [*Turnbull et al.*, 2015]. This can lead to a large seasonal cycle in δ_{source}that may be representative of larger scale processes (>100 km^2) and susceptible to nonlocal fossil fuel emissions. The use of a nearly collocated background provided a seasonal pattern of δ_{source} that was generally robust to small changes in background location relative to the site observations. For example, the seasonal pattern of δ_{source} at SGP and Rannells (both mixed C_3/C_4) was similar, yet the background location for SGP was much more separated from the site observations than Rannells Prairie (Table 2, Figure 4). Furthermore, the pattern of smoothed δ_{source} at *US-NR1* was similar when calculated from the data taken from each of the nine tower inlet heights separately (Figure S7).

The seasonal amplitude in isoforcing at the sites was driven primarily by seasonal changes in land-atmosphere net carbon exchange (e.g., net carbon uptake to land in the summer, net carbon release to atmosphere in the winter) and *not* from seasonal changes in δ_{source}(Figure 9, section 3.5). Therefore, NEE was more important than δ_{source} in shaping seasonal patterns in local δ_{atm} at our sites. Fossil fuel emissions in Salt Lake City had the largest multiyear impact upon local δ_{atm} because of the most negative isoforcing (^{13}C depleted $CO_2$to the atmosphere) of any site. Negative isoforcing from urban centers contributes to long-term global decrease in δ_{atm} (Suess effect). Our estimate of seasonal isoforcing in Salt Lake City did not account for biogenic influence although it has a small but nonnegligible influence on local δ_{atm} [*Pataki et al.*, 2003a]. As a result, the isoforcing (Figure 9) is likely underestimated during the summer (net carbon biogenic uptake) and overestimated in the fall (net carbon biogenic release). On a seasonal basis, the vegetated sites (especially Harvard) had the largest change in isoforcing. This

large change in seasonal isoforcing, combined with a range of timing in peak isoforcing among the plant functional types represented by the sites (Figure S6), suggests a linkage between the generation of ^{13}C enriched CO_2 (positive isoforcing) and delayed response of δ_{atm} due to mixing time. We caution that this suggestion of cause and effect is based on a subset of sites within the midlatitudes and does not include any quantification of the seasonal isoforcing impact from the ocean or land-atmosphere disequilibrium, which are important in closing the annual atmospheric ^{13}C budget [*Randerson et al.*, 2002; *Bowling et al.*, 2014] and explaining interannual variation in δ_{atm} [*Alden et al.*, 2010; *van der Velde et al.*, 2013]. However, on *seasonal* timescales, the land carbon exchange in the Northern Hemisphere drives the seasonal pattern in atmospheric CO_2 [*Keeling et al.*, 1996] and δ_{atm}.

4.3 Comparison With Discrimination Derived From Tree Ring Analysis

Similar to *Ballantyne et al.* [2010], we used tree ring measurements as an independent way to verify the seasonal changes of δ_{source} derived from atmospheric mixing models (e.g., Figure 4). Our results for seasonality of δ_{source} for forest sites are generally consistent with discrimination estimates derived from $\delta^{13}C$ of cellulose in the wood of tree rings (δ_{wood}) at other midlatitude forested sites similar to the ones studied here. The amplitudes of $\delta_{wood}$and δ_{source} should be proportional, although not equivalent to each other for two reasons. First, δ_{source} is influenced by photosynthetic fractionation (δ_{photo}) and a variety of post-photosynthetic fractionation processes [*Bowling et al.*, 2008; *Brüggemann et al.*, 2011]. The δ_{wood} signature, on the other hand, is influenced by photosynthetic fractionation and fractionation during wood growth. Second, the carbon allocated to tree rings is not only the transfer of recent carbon assimilated from photosynthesis but a combination of both recent assimilate and stored carbon [*Gessler et al.*, 2014]. Therefore, the seasonal amplitude of δ_{source} should be larger than that of δ_{wood}. For example, a single substrate model [*Ogée et al.*, 2009] suggests a ~30% reduction in amplitude between the seasonal range of δ_{photo} and δ_{wood}. Observations support the idea that there is a reduction in the seasonal ranges of δ_{photo} to δ_{wood} of about 50% for deciduous species [*Helle and Schleser*, 2004; *Offermann et al.*, 2011] and 30% for conifer [*Gessler et al.*, 2009]. The closer match between the seasonal range of δ_{photo} to δ_{wood} of coniferous species is consistent with the finding that the dynamics of storage and remobilization of carbon are less pronounced for these species [*Gessler et al.*, 2014]. Thus, seasonal changes in the $\delta^{13}C$ of assimilated carbon (driven by photosynthetic fractionation) are more likely to directly imprint on seasonal changes in δ_{wood}. Observations of the seasonal amplitude of δ_{wood} include the species *Pinus taeda* (1–2‰) [*Ballantyne et al.*, 2010], *Pinus ponderosa* (1‰) [*Leavitt et al.*, 2002], *Pinus radiata* (4‰)

[*Barbour et al.*, 2002], *Pinus sylvestris* (1.5‰) [*Gessler et al.*, 2009], *Fagus sylvatica* (1.3‰) [*Offermann et al.*, 2011], *Populus nigra* (2.5‰), and *Quercus petraea* (1.3‰) [*Helle and Schleser*, 2004]. Assuming a 30% reduction in amplitude between δ_{photo} to δ_{wood}, the relatively small growing season amplitude in δ_{source} (2.3‰) in our analysis is consistent with the observed seasonal amplitude of δ_{wood} (1.6‰). Furthermore, the mismatch between the amplitude of seasonal cycle of δ_{source} (3‰) and δ_{wood} (1‰) at a pine forest in North Carolina [*Ballantyne et al.*, 2010] is consistent with an overestimation of δ_{source} using remote-background mixing model methodology (see section 4.4).

4.4 Impact of Mixing Model Methodology on δ_{source}

Previous analyses [e.g., *Ballantyne et al.*, 2010, 2011] may have overestimated the seasonal amplitude of δ_{source} by not accounting for either regional changes in background air, or for short duration, high frequency fossil fuel contamination events. At *US-NR1*, for example, we suspected that the seasonal amplitude of δ_{source} was overestimated due to the influence from urban emissions [*Bowling et al.*, 2014]. Two lines of evidence support this. First, we found a large seasonal amplitude of δ_{source} at *US-NR1* when using the *smoothed* approach, but the seasonal amplitude was negligible when using the *nonsmoothed* approach (Figure 5; section 3.2). Second, when time periods with urban influence were removed (based on analysis of anthropogenic trace gases; Figure 6; section 3.3), the resulting δ_{source} was more enriched (Figure 7). Inclusion of only the urban-influenced periods led to a δ_{source} that was too depleted (−32‰ thru −30‰) to be biogenic in origin [*Schaeffer et al.*, 2008; *Hu et al.*, 2010b] and was characteristic of $\delta^{13}C$ of fossil fuel combustion (natural gas: −38, petroleum: −28) [*Bush et al.*, 2007]. Niwot Ridge likely experiences urban contamination from the Denver-Boulder metropolitan area [*Roberts et al.*, 1985; *Parrish et al.*, 1991]. *SGP*, however, was not susceptible to winter underestimation of δ_{source} when using the *smoothed* approach (Figure 5) for two possible reasons. First, anthropogenic emissions may not be as prevalent near *SGP*. Whereas *US-NR1* is only ~30 km to the west of Boulder and ~60 km to the northwest of downtown Denver, the closest major urban centers to *SGP* (Oklahoma City, Tulsa) are approximately 170 km to the south and southeast of *SGP* which may allow for more mixing and dilution of the urban air. Second, during the winter months, *SGP* provides a greater biological signal (land sink of carbon: 0.54 μmol m^{-2} s^{-1}) than *US-NR1* (land source of carbon: 0.33 μmol m^{-2} s^{-1}; Figure 9) that may help constrain the δ_{source} regression. The increased carbon sink at *SGP* is likely from a combination of a warmer winter climate as compared to *US-NR1* and the planting and fertilization of winter wheat (October to May) during most years between 2003 and 2012 [*Raz-Yaseef et al.*, 2015]. On

average, there is no photosynthesis at US-NR1 between mid-November and late March [*Raczka et al.*, 2016].

We note that mixing models can provide spurious δ_{source} when atmospheric measurements are influenced by multiple CO_2 sources with distinct $\delta^{13}C$ signatures [*Vardag et al.*, 2016]. We combined all day and night flask data into a single regression in an effort to maximize the sample size in an effort to best constrain the regression used to calculate δ_{source}. Strictly speaking, using daytime flask observations combines two separate CO_2 sources/sinks (photosynthesis, ecosystem respiration) with distinct but similar $\delta^{13}C$ (δ_{photo}, δ_{resp}). The difference between δ_{photo} and δ_{resp} is estimated to be ~1‰ at *US-NR1* [*Bowling et al.*, 2014] and 0.5‰ at Harvard [*Wehr and Saleska*, 2015]. We found that using all the atmospheric data was justified because calculating the δ_{source} for the day and night observations separately did not provide a significant difference in the seasonal amplitude for *US-NR1* [*Bowling et al.*, 2014], Harvard, and SGP [*Torn et al.*, 2011]. At *US-NR1*, day-only data led to poorer monthly regressions as compared to night-only data, but for most months, the difference was small ($R^2 < 0.1$) [*Bowling et al.*, 2014]. The strongest indicator of regression quality for *US-NR1* was season. With little biological activity and only minimal temporal variation in CO_2 and $\delta^{13}C$, monthly regressions during the winter (October–March) were relatively poor ($R^2 < 0.85$); however, the months most relevant for comparison between VPD and δ_{source} (April–September; Figure 8) had $R^2 > 0.85$ [*Bowling et al.*, 2014].

5 Conclusions

We used atmospheric measurements of CO_2 and $\delta^{13}C$ at a variety of sites across the United States representing major vegetation types and an urban area to examine what drives the seasonal pattern of the $\delta^{13}C$ of land-atmosphere exchange (δ_{source}). We found that seasonal changes in VPD at the forest sites were not responsible for the seasonal changes in δ_{source}, with the exception of Wind River, where a unique combination of seasonal drought and stand-age effects likely played a role. Although the grassland sites showed a correlation between δ_{source} and VPD, this was more likely driven by a shift in relative productivity between the C_3/C_4 species during the summer. The grassland and urban sites showed the largest seasonal change in δ_{source} due to the C_3/C_4 grass growth transition and the type/intensity of fossil fuel emissions, respectively. The largest driver of seasonal patterns in local δ_{atm} was the seasonal change of net carbon uptake, especially for forest sites, and *not*the relatively small seasonal variation in δ_{source} (0.5‰). Overall, the lack of correlation between VPD and δ_{source} suggests that stomatal response to VPD is not the main cause of the coherent global seasonal cycle of δ_{source} and that C_3/C_4 grasslands are more likely to play a dominant role within the midlatitudes. Although natural mixtures of C_3/C_4 grasslands as analyzed here are increasingly rare due to agricultural conversion, the impact upon the atmosphere of

regional patchwork of C_3 and C_4 croplands is likely similar due to atmospheric mixing. This site-specific information on δ_{source} can help formulate and calibrate the relationship between atmospheric moisture, stomatal conductance, and ^{13}C discrimination within terrestrial carbon models by excluding regional and continental scale influence from local analyses. Such models can be used to better quantify the contributions of the three key mechanisms (stomatal response to VPD, variation in C_3/C_4 productivity, and fossil fuel emissions) that influence the seasonal variation in δ_{source}.

These findings demonstrate that the location used to account for atmospheric background variation plays a critical role in the estimation of δ_{source} and what it represents. The choice of background location should depend on whether the intent is to understand localized site-level mechanisms or the regional, integrated, impact of the landscape on δ_{source}. More studies are required to understand the difference between regional and local estimations of δ_{source} and to determine whether this difference is caused by the spatial scale of the vegetated landscape or the influence of anthropogenic emissions.

Acknowledgments

Thank you to Ashley Ballantyne for helpful discussion regarding the mixing model methods, interpretation of results, and helpful comments on a manuscript draft. Thanks to the AmeriFlux site investigators for sharing the flux tower data, including Sonia Wharton who provided flux tower data and discussion for the Wind River site. Thanks to Ed Dlugokencky and Paul Novelli for providing the flask observations from the Niwot Ridge tundra site. The authors thank Daniel Mendoza of the University of Utah who provided Hestia fossil fuel emissions data for Salt Lake City. Thank you to Ryan Bares who helped with the collection and organization of the Salt Lake City isotope data. The support and resources from the Center for High Performance Computing at the University of Utah are gratefully acknowledged. This research was supported by the US Department of Energy (DOE), Office of Science, Office of Biological and Environmental Research, Terrestrial Ecosystem Science (TES) Program under award number DE-SC0010625, and the US National Science Foundation Macrosystems Biology Program under award EF-1137336. Additional support was provided by the Atmospheric Radiation Measurement Program (ARM) under award number DE-AC02-05CH11231 and through the NOAA Climate Program Office's Atmospheric Chemistry, Carbon Cycle, and Climate Program, grant NA14OAR4310178. Funding for AmeriFlux data resources and operation of the sites was provided by the U.S. Department of Energy's Office of Science. Harvard Forest is an AmeriFlux core site also supported by NSF as part of the Harvard Forest LTER. The laser spectrometer

measurements at the Harvard Forest were supported by the DOE TES program under award DE-SC0006741. The location of the data sets used for the analysis is given in the methods of this manuscript (sections 2.1–2.4).